Arch Microbiol (1999) 171 : 371–385

ORIGINAL PAPER

Albert A. De Graaf · Katharina Striegel
Rolf M. Wittig · Birgit Laufer · Günter Schmitz
Wolfgang Wiechert · Georg A. Sprenger
Hermann Sahm

Metabolic state of *Zymomonas mobilis* in glucose-, fructose-, and xylose-fed continuous cultures as analysed by ^{13}C- and ^{31}P-NMR spectroscopy

Received: 7 January 1999 / Accepted: 22 March 1999

Abstract The reasons for the well-known significantly different behaviour of the anaerobic, gram-negative, ethanologenic bacterium *Zymomonas mobilis* during growth on fructose (i.e. decreased growth and ethanol yields, increased by-product formation) as compared to that on its second natural substrate, glucose, have remained unexplained. A xylose-fermenting recombinant strain of *Z. mobilis* that was recently constructed in our laboratory also unexpectedly displayed an increased formation of by-products and a strongly reduced growth rate as compared to the parent strain. Therefore, a comprehensive study employing recently developed NMR-based methods for the in vivo analysis of intracellular phosphorylated pool sizes and metabolic fluxes was undertaken to enable a global characterization of the intracellular metabolic state of *Z. mobilis* during growth on ^{13}C-labelled glucose, fructose and xylose in defined continuous cultures. The ^{13}C-NMR flux analysis indicated that ribose 5-phosphate is synthesized via the nonoxidative pentose phosphate pathway in *Z. mobilis*, and it identified a metabolic bottleneck in the recombinant xylose-fermenting *Z. mobilis* strain at the level of heterologous xylulokinase. The ^{31}P-NMR analyses revealed a global alteration of the levels of intracellular phosphorylated metabolites during growth on fructose as compared to that on glucose. The results suggest that this is primarily caused by an elevated concentration of intracellular fructose 6-phosphate.

A. A. De Graaf (✉) · K. Striegel · B. Laufer · G. Schmitz
G. A. Sprenger · H. Sahm
Institut für Biotechnologie I, Forschungszentrum Jülich,
D-52425 Jülich, Germany
e-mail: a.de.graaf@fz-juelich.de,
Tel.: +49-2461-613969, Fax: +49-2461-612710

R. M. Wittig
Alfred-Wegener-Institut für Polar- und Meeresforschung,
Postfach 120161, D-27515 Bremerhaven, Germany

W. Wiechert
IMR, Abteilung Simulationstechnik, Universität Siegen,
D-57068 Siegen, Germany

Key words *Zymomonas mobilis* · Metabolic flux analysis · Sugar phosphates · Glucose · Fructose · Xylose · ^{13}C-NMR · In vivo ^{31}P-NMR · Rate-limiting step

Abbreviations *ED* Entner-Doudoroff · *PPP* Pentose phosphate pathway · *GND* 6-Phosphogluconate dehydrogenase · *PGI* Phosphoglucose isomerase · *PRE* Ribulose-5-phosphate epimerase · *PRI* Phosphoribose isomerase · *TAL* Transaldolase · *TKT* Transketolase · *XI* Xylose isomerase · *XK* Xylulokinase · *AcCoA* Acetyl-CoA · *AKG* 2-Oxoglutarate · *E4P* Erythrose 4-phosphate · *F6P* Fructose 6-phosphate · *G6P* Glucose 6-phosphate · *GAP* Glyceraldehyde-3-phosphate · *KDPG* 2-Keto-3-deoxy-6-phosphogluconate · *OAA* Oxaloacetate · *PEP* Phospho*enol*pyruvate · *PGA* Phosphoglycerate · *PYR* Pyruvate · *RI5P* Ribose 5-phosphate

Introduction

Zymomonas mobilis is an anaerobic, gram-negative bacterium that produces ethanol from glucose via the Entner-Doudoroff [2-keto-3-deoxy-6-phosphogluconate (KDPG)] pathway in conjunction with the enzymes pyruvate decarboxylase and alcohol dehydrogenase. The organism only grows on glucose, fructose and sucrose. Although the pathways for glucose and fructose degradation are almost identical (they differ only in the transport and first two steps), growth and ethanol yields on fructose are lower than on glucose, while the synthesis of by-products, especially glycerol and dihydroxyacetone, is increased (Dawes and Ribbons 1966; Viikari and Korhola 1986; Viikari 1988; Struch 1992). The action of a possible aldolase side-activity selectively cleaving fructose to dihydroxyacetone and glyceraldehyde-3-phosphate could be ruled out (Horbach et al. 1994). Also, while the affinity of the glucose facilitator of *Z. mobilis* is almost tenfold lower for fructose (K_m = 39 mM) than for glucose (K_m = 4.1 mM) (Weisser et al. 1995, 1996), it has an approximately equal V_{max} for glucose and fructose. Therefore, no significant differences in glucose and fructose metabolism due to the facilitator

characteristics alone can be expected either in batch cultures (where the substrate concentration is much higher than the K_m) or in chemostat cultures (where the specific substrate uptake rate at a given dilution rate is approximately equal for glucose and fructose). Unfortunately, no comparative studies providing comprehensive information on intracellular metabolite concentrations during glucose and fructose metabolism have been reported to date.

The glucose facilitator in *Z. mobilis* has also been shown to transport xylose very efficiently in this organism (Schoberth and De Graaf 1993; Weisser et al. 1996), with K_m = 40 mM and the V_{max} twice as high as for glucose (Weisser et al. 1996). However, the *Z. mobilis* wild-type is not able to grow on this substrate due to the lack of catabolic enzymes (Feldmann et al. 1992 a). Much effort has been put into attempts to give *Z. mobilis* a xylose-degrading capacity via recombinant DNA techniques. This would potentially render this organism suited for industrial ethanol fuel production from low-cost substrates in agricultural residues. Feldmann et al. (1992 a) have succeeded in introducing heterologous genes from *Escherichia coli* for transketolase, transaldolase, xylose isomerase and xylulokinase. Zhang et al. (1995) were the first to construct a functional recombinant xylose-fermenting *Z. mobilis* strain. In a similar approach, using the genes for xylose isomerase and xylulokinase from *Klebsiella pneumoniae* in addition to the genes for transketolase and transaldolase from *E. coli*, a xylose-degrading *Z. mobilis* recombinant strain has also been successfully constructed in our laboratory (Laufer 1998). However, although both strains were able to grow on xylose and to produce ethanol at a yield as high as 0.44 g/g xylose, i.e. 86% of the theoretical yield, specific growth and production rates were four- to fivefold lower than those typically observed on glucose. As with fructose, the cause for this strong impairment of growth and productivity is still unknown, but it has been speculated (Zhang et al. 1995) that the pathway control structure may resist a radical alteration of metabolic flux distribution such as is necessary for xylose metabolism in *Z. mobilis*.

In the past few years, powerful methods for metabolic flux analysis using metabolite balancing together with ^{13}C stable isotope labelling and NMR spectroscopy have been developed (Wiechert and De Graaf 1996, 1997; Wiechert et al. 1997) and successfully applied, e.g. in the study of *Corynebacterium glutamicum* metabolism (Marx et al. 1996, 1997). These methods allow the quantitation of all in vivo fluxes in the bacterial primary metabolism in defined stationary conditions by analysing ^{13}C-labelling patterns in proteinogenic amino acids extracted from cells grown in the presence of labelled substrates. The metabolic state of the cells can also be directly assessed by in vivo ^{31}P-NMR (Gadian 1995). This technique has been successfully applied to monitor the concentrations of intracellular metabolites in *Z. mobilis* during glucose catabolism (Barrow et al. 1984; Strohhäcker et al. 1993). Whereas these studies required the use of extremely dense cell suspensions, resulting in poorly defined physiological conditions, newly developed integrated in vivo NMR/fermentor systems allow the study of baceria under well-defined conditions in continuous culture (De Graaf et al. 1992; Hartbrich et al. 1996; Weuster-Botz and De Graaf 1996).

It was the purpose of the present study to apply metabolic flux analysis and the newest in vivo ^{31}P-NMR techniques in order to elucidate the reasons for the different growth yields, by-product spectra and glycolytic rates as observed during glucose and fructose metabolism in *Z. mobilis* CP4 as well as during xylose metabolism in a xylose-degrading recombinant Z. *mobilis* strain (Laufer 1998).

Materials and methods

Bacterial strains, plasmids and growth conditions

Z. mobilis CP4 (ATCC 31821) was used for all experiments with glucose and fructose as substrate. *Z. mobilis* CP4/pZY228/pZY557*tal* (described below) was used for the experiment with xylose as substrate.

The three cultivation media (I, II and III) for isotope-labelling-based metabolic flux analysis contained (per litre):

1. Medium I: 70 g D-glucose (mixture of 80% unlabelled glucose and 20% [2-^{13}C]glucose; Omicron Biochemicals, South Bend, IN, USA), 0.87 g NH_4Cl, 0.082 g $MgSO_4 \times 7H_2O$, 0.18 g KH_2PO_4, 0.125 g trisodium citrate, 0.0021 g $FeSO_4 \times 7H_2O$, 1 mg Ca-panthotenate and 1 mg biotin.

2. Medium II: 70 g D-fructose (mixture of 80% unlabelled fructose and 20% [2-^{13}C]fructose; Omicron Biochemicals), 1.6 g NH_4Cl, 1.0 g $MgSO_4 \times 7H_2O$, 3.5 g KH_2PO_4, 0.21 g trisodium citrate, 0.010 g $FeSO_4 \times 7H2O$, 1 mg Ca-panthotenate and 1 mg biotin.

3. Medium III: 70 g D-xylose (mixture of 81% unlabelled xylose and 19% [1-^{13}C]xylose; Cambridge Isotope Laboratories, Cambridge, Mass., USA), 1.98 g $(NH_4)_2SO_4$, 1.0 g $MgSO_4 \times 7H_2O$, 3.48 g KH_2PO_4, 0.21 g trisodium citrate, 0.010 g $FeSO_4 \times 7H_2O$ and 10 ml of a vitamin stock solution containing (per litre) 1.65 mg biotin, 150 mg choline, 0.05 mg cyanocobalamin, 0.5 mg folic acid, 0.7 mg inositol, 299 mg nicotinic acid, 382 mg *p*-aminobenzoic acid, 137 mg panthotenic acid, 21.6 mg pyridoxine, 58.3 mg riboflavin and 265 mg thiamine. Thus added, the fermentation medium contained vitamins in concentrations equivalent to those present in 5 g/l bacto-yeast-extract (according to the supplier: Difco, Detroit, Mich., USA). The medium contained 1 mM isopropyl-β-D-thiogalactopyranoside (IPTG) (Biomol, Hamburg, Germany) for induction of heterologous enzymes and 100 mg chloramphenicol/l, 15 mg tetracycline /l and 40 mg nalidixic acid/l for strain selection (Laufer 1998).

In all media, the pH was adjusted to 5.8 with KOH. Vitamins were added after sterile filtration. The sugar was autoclaved separately before addition.

Cultures (300-ml volume) were inoculated with cells grown anaerobically overnight in a medium containing per litre: 10 g yeast extract, 1 g KH_2PO_4, 1 g $(NH_4)_2SO_4$, 0.5 g $MgSO_4 \times 7H_2O$ and 20 g of the respective sugar. Cultures were purged with argon at a controlled rate of 20 l/h (mass flow controller; Brooks Instruments, Veenendaal, The Netherlands) to maintain anaerobiosis. After reaching a biomass concentration of approximately 1.5 g dry wt./l (0.7 g dry wt./l for the xylose experiment) in the initial batch growth phase, chemostat operation was started with unlabelled substrate. Dilution rates were 0.1 h^{-1} for the glucose and fructose experiments, and 0.018 h^{-1} for the xylose experiment. After reaching the steady state (as judged from OD_{550} measurements) after approximately three dilution times, the feed was changed to the labelled substrate mixture. The temperature was controlled at 30 °C,

and the pH was kept at 5.8 using NaOH. The cells were harvested after chemostat operation for another five dilution times, thus enabling more than 99% dilution of initial unlabelled biomass.

In vivo ^{31}P-NMR experiments were carried out on high-cell-density continuous cultures growing on glucose or fructose, using a recently developed membrane cyclone bioreactor system (Hartbrich et al. 1996). The media contained per litre: 130 g glucose or fructose, 250 mg KH_2PO_4, 1,230 mg NH_4Cl, 140 mg $MgSO_4 \times 7H_2O$, 235 mg citric acid (monohydrate), 3 mg $FeSO_4 \times 7H_2O$, 1.1 mg biotin, 1.1 mg Ca-pantothenate and 0.35 mg antifoam agent (Dehysan Z211; Henkel, Düsseldorf, Germany). The mineral salts and the sugar together with the antifoam agent were autoclaved separately. After mixing these compounds, Ca-pantothenate and biotin were added in a filtration-sterilized form. A 48-h precultivation was carried out in a stirred 1-l flask (500 ml culture medium, 5% inoculum). After transfer of the preculture into the membrane cyclone bioreactor, a 24-h batch operation was carried out without filtrate flow prior to the start of continuous cultivation in the corresponding operation mode. The reactor temperature was controlled at 30 °C (pH 5.9) The dilution rates of the medium and the biomass were independently set to 0.455 h^{-1} and 0.023 h^{-1}, respectively, by adjusting the medium, bleed and filtrate flows of the system.

Recombinant DNA techniques

The cloning of the *talB* gene of *E. coli* K-12 on plasmid pGSJ451 has been described earlier (Sprenger et al. 1995 b). A 1.0-kb DNA fragment containing the entire *talB* gene was generated by digestion with *Sph*I and was ligated to vector pZY557, a derivative of plasmid pZY507 (Reipen et al. 1995; G. A. Sprenger, unpublished work) that was cleaved likewise. Transformation and selection for chloramphenicol resistance yielded plasmid pZY557*tal* with the *talB* gene under the control of an IPTG-regulated *tac*promotor (Reipen et al. 1995). After introduction in the mobilizing *E. coli* strain S17-1 (Simon et al. 1983), conjugation with *Z. mobilis* strain CP4/pZY228 (Feldmann et al. 1992a) yielded strain CP4/pZY228/pZY557*tal*, which expressed heterologous activities of xylose isomerase, xylulokinase, transketolase and transaldolase. After selection for xylose-utilizing strains, a clone was obtained that allowed rapid conversion of xylose to ethanol and carbon dioxide (Laufer 1998).

Preparation of crude extracts

Cell-free extracts for enzyme determinations were prepared as described previously (Feldmann et al. 1992 a). Cell-free extracts for metabolite determinations by ^{31}P-NMR spectroscopy were prepared as follows: in order to quench the metabolism instantaneously, 60 ml of cell suspension from the membrane cyclone bioreactor was injected into 180 ml 60% methanol precooled to –40 °C by addition of liquid nitrogen. The mixture, then at –20 °C, was cooled down to –30 °C and then centrifuged (5,000 *g*, 5 min, –20 °C) in a centrifuge precooled to –20 °C. The cell pellet was introduced in 8 ml chloroform (–20 °C). Under heavy stirring, 5 ml of buffer solution [2 mM Pipes, 50 mM EDTA (pH 7.2)] was added, and the suspension was stirred for 30 min at –10 °C. After centrifugation (3,000 *g*, 10 min, –20 °C), the water and chloroform phases were separated. The procedure was repeated after adding another 5 ml of buffer to the chloroform phase. Both supernatants were combined, neutralized and lyophilized, and were then kept at –20 °C until NMR analysis. Prior to NMR analysis, the lyophilisate was dissolved in 2 ml buffer [75 mM Tris-HCl, 150 mM EDTA (pH 8.30)], and 30 µl triethylphosphate and 450 µl D_2O were added. The volume was adjusted to 3.0 ml with distilled water, and the sample was transferred to a 10-mm NMR tube. Triethyl phosphate was used as chemical shift standard resonating at 0.44 ppm relative to 85% H_3PO_4 (Kirk et al. 1986). Resonance assignments were confirmed by addition of the pure standards.

Enzyme assays

Xylose isomerase (EC 5.3.1.5) was assayed discontinuously as described previously (Feldmann et al. 1992 b). This assay measured xylulose (formed from xylose) with sorbitol dehydrogenase. Xylulokinase (EC 2.7.1.17) was measured according to Simpson (1966). The assay mixture contained in a final volume of 1.0 ml: 50 mM Tris-HCl (pH 7.8), 50 mM KCl, 1.0 mM EDTA, 5.0 mM $MgCl_2$, 1.0 mM phospho*enol*pyruvate, 50 µl 1.0 mM D-xylulose, 0.09 mM NADH, 20–100 µl crude extract, 0.1 U lactate dehydrogenase, 0.022 U pyruvate kinase and 0.5 mM ATP. Transaldolase (EC 2.2.1.2) was measured in an assay modified from Tsolas and Horecker (1972). The assay contained per millilitre: 87 mM triethanolamine (pH 8.5), 17 mM EDTA, 4.2 mM fructose 6-phosphate, 0.38 mM NADH, 30 µg glycerol-3-phosphate dehydrogenase/triose phosphate isomerase, 10–50 µl crude extract and 0.6 mM erythrose 4-phosphate. Transketolase (EC 2.2.1.1) was determined according to Sprenger et al. (1995 a). Phosphoglucoseisomerase (EC 5.3.1.9) was assayed according to Algar and Scopes (1985) in an assay containing per millilitre: 27 mM K-Mes (pH 6.5), 45 mM KCl, 1.8 mM $MgSO_4$, 0.09 mM EDTA, 0.18 mg bovine serum albumin, 1 mM fructose 6-phosphate, 10–50 µl crude extract, 1.75 U glucose-6-phosphate dehydrogenase and 0.5 mM $NADP^+$.

Analytical methods

Analysis of metabolites in culture supernatant

Ethanol, acetate, acetoine and acetaldehyde were quantitated by GC analysis (GC series 5890; Hewlett Packard, Waldbronn, Germany) using a Porapak QS 80–100 mesh column. Sorbitol, lactate and glycerin were determined enzymatically (Boehringer, Mannheim, Germany). Xylitol, xylulose and residual xylose were determined by HPLC (Merck-Hitachi) equipped with an RI detector ERC 93087 (Alteglofsheim, Germany) using an Aminex HPX 87C 300 mmx, 7.8-mm column (BioRad, Munich, Germany).

Analysis of metabolites in culture gas

The fermentor gas was continuously monitored for ethanol (BINOS 1 for C_2H_5OH; Leybold Heraeus/Fisher Rosemount, Hanau, Germany) and carbon dioxide (CO_2 BINOS 100 M; Fisher Rosemount, Hanau, Germany) contents to quantitate the amounts of these compounds evaporated from the culture.

Preparation of labelled biosynthetic monomers for NMR spectroscopy

The preparation and purification of amino acids from the cell protein and guanosine derivates from the cell RNA were done as described previously (Marx et al. 1996, 1997).

^{1}H-NMR spectroscopy

The ^{13}C fractional enrichments in protonated carbons of the purified nucleotides and amino acids were determined by ^{1}H-NMR as described previously (Marx et al. 1996). The ^{13}C fractional enrichments in nonprotonated carbons were determined using heteronuclear spin-echo difference spectroscopy (Wendisch et al. 1997).

In vivo ^{31}P-NMR spectroscopy

In vivo ^{31}P-NMR spectroscopy was performed on high-cell-density cultures at a measuring frequency of 162.0 MHz using 90°

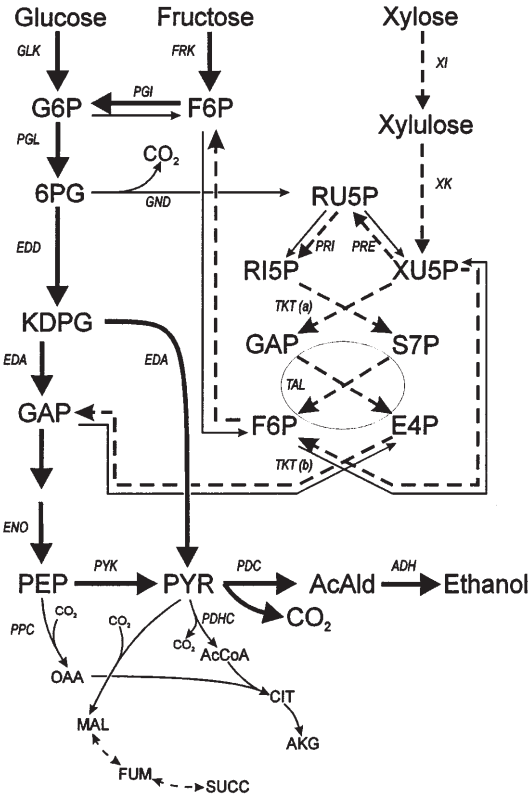

Fig. 1 Scheme of *Zymomonas mobilis* principal metabolic pathways for the metabolism of glucose, fructose (*solid lines*) and xylose (*broken lines*). The involved enzymes are denoted by the following three-letter codes: *GLK* glucokinase, *FRK* fructokinase, *PGI* phosphoglucose isomerase, *PGL* phosphogluconolactonase, *GND* 6-phosphogluconate dehydrogenase, *EDD* 6-phosphogluconate dehydratase, *EDA* 2-keto-3-deoxy-gluconate aldolase, *ENO* enolase, *PYK* pyruvate kinase, *PPC* phospho*enol*pyruvate carboxylase, *PDC* pyruvate decarboxylase, *PDHC* pyruvate dehydrogenase complex, *ADH* alcohol dehydrogenases I and II, *XI* xylose isomerase, *XK* xylulokinase, *PRE* ribulose-5-phosphate epimerase, *PRI* phosphoribose isomerase, *TKT* transketolase [*(a)* and *(b)* merely denote the two different reactions shown], and *TAL* transaldolase. *XI*, *XK* and *TAL* are absent from wild-type *Z. mobilis*, but the heterologous enzymes (in addition to heterologous *TKT*) are present in the xylose-degrading strain *Z. mobilis* CP4/pZY228/pZY557*tal* used in this study. Metabolites are denoted by: *G6P* glucose 6-phosphate, *F6P* fructose 6-phosphate, *6PG* 6-phosphogluconate, *KDPG* 2-keto-3-deoxy-6-phosphogluconate, *GAP* glyceraldehyde-3-phosphate, *PEP* phospho*enol*pyruvate, *PYR* pyruvate, *RU5P* ribulose 5-phosphate, *RI5P* ribose 5-phosphate, *XU5P* xylulose 5-phosphate, *S7P* sedoheptulose 7-phosphate, *E4P* erythrose 4-phosphate, *AcAld* acetaldehyde, *OAA* oxaloacetate, *AcCoA* acetyl-coenzyme A, *CIT* citrate, *AKG* 2-oxoglutarate, *MAL* malate, *FUM* fumarate, and *SUCC* succinate

pulses (45 μs), a repetition time of 55 ms, and a total measurement time of 75 min per spectrum. Further details of the NMR measurement methods and quantitation procedures used have been described previously (Hartbrich et al. 1996).

^{31}P-NMR spectroscopy of cell-free extracts

For chloroform extracts, proton-decoupled ^{31}P-NMR measurements at 162.0 MHz were performed. Per spectrum, 1,800 scans with 60° pulses were acquired in 2 h at 25 °C as described previously (Strohhäcker et al. 1993).

Flux modeling

The flux model (Fig. 1) comprised the generally accepted pathways of primary metabolism for *Z. mobilis*, e.g as described by Sprenger (1996). *Z. mobilis* typically catabolizes more than 95% of the carbohydrate carbon via the Entner-Doudoroff pathway. In the wild-type, the pentose phosphate pathway is incomplete (Feldmann et al. 1992 a; Zhang et al. 1995), with high activities of ribose-5-P isomerase and ribulose-5-P epimerase, weak activities of 6-phosphogluconate dehydrogenase and transketolase, and no detectable activity of transaldolase, which, however, is dispensible in biosynthetic pathways during growth on hexoses (Feldmann et al. 1992 a). The organism lacks a complete citric acid cycle but is able to synthesize 2-oxoglutarate from pyruvate via acetyl-CoA, citrate and isocitrate (Dawes et al. 1970; Bringer-Meyer and Sahm 1993). Phospho*enol*pyruvate carboxylase and malic enzyme provide additional anaplerotic reactions (Bringer-Meyer and Sahm 1989).

In the xylose-degrading recombinant strain, the following additional heterologous enzymes in the pentose phosphate branch are present (see Fig. 1): xylose isomerase, xylulokinase, transaldolase and transketolase.

The principal routes of the [2-^{13}C] label from glucose and fructose are depicted in Fig. 2. No principal differences in the labelling patterns between glucose and fructose metabolism can be expected. Via the Entner-Doudoroff pathway, pyruvate resulting from cleavage of KDPG is labelled in C-2, while unlabelled glyceraldehyde-3-phosphate via phospho*enol*pyruvate (PEP) leads to unlabelled pyruvate. Thus, ethanol is expected, with a fractional labelling of its C-1 equal to half the original labelling of glucose or fructose. Ribose 5-phosphate can be synthesized from 6-phosphogluconate via the oxidative pentose phosphate pathway and ribose-5-phosphate isomerase, in which case it is labelled in C-1, or alternatively from fructose 6-phosphate via the transketolase reaction of the nonoxidative pentose phosphate pathway, ribulose-5-phosphate epimerase and ribose-5-phosphate isomerase, in which case the label resides in C-2 of ribose 5-phosphate. Thus, the labelling of ribose 5-phosphate, which after RNA hydrolysis can be retrieved, for example, from guanosine (Marx et al. 1997), is a sensitive marker of the flux distribution over the oxidative and the nonoxidative pentose phosphate pathways.

The labelling patterns expected from [1-^{13}C]xylose in the recombinant strain show more variety (Fig. 3). Stoichiometry of the pentose phosphate pathway predicts that two molecules of fructose 6-phosphate and one molecule of glyceraldehyde-3-phosphate will be produced from three molecules of xylose. The glyceraldehyde-3-phosphate molecule will be unlabelled; one of the fructose 6-phosphate molecules will be labelled on the C-1, while the other will be labelled on both the C-1 and the C-3. From these precursors, a total of five molecules of pyruvate will be produced: one labelled on C-1, another labelled on both C-1 and C-3, and three unlabelled. Thus, ethanol is expected to be labelled in C-2 with 20% of the original label in xylose. CO_2 is expected to be labelled twice as high. Possible activity of the oxidative pentose phosphate pathway will be reflected in a labelling of C-3 of ribose 5-phosphate (Fig. 3).

Experimental data for the positional labelling of intracellular ribose 5-phosphate, glyceraldehyde-3-phosphate, PEP, erythrose 4-phosphate, pyruvate, oxaloacetate, 2-oxoglutarate and CO_2 were obtained from their respective products guanosine, cytidine, serine, glycine, phenylalanine, alanine, valine, leucine, aspartate, threonine, glutamate and arginine purified after biomass hydrolysis as described above. These data, together with measured rates for substrate uptake and (by-)product excretion as well as calculated precursor fluxes for biomass synthesis were used for a comprehensive flux analysis. The set of fluxes yielding a minimum deviation between simulation and measurements of the fractional ^{13}C enrichments and the measurable rates was taken as the best estimate for the intracellular flux distribution. The computational details of this procedure are described elsewhere (Marx et al. 1996; Wiechert and De Graaf 1997; Wiechert et al. 1997).

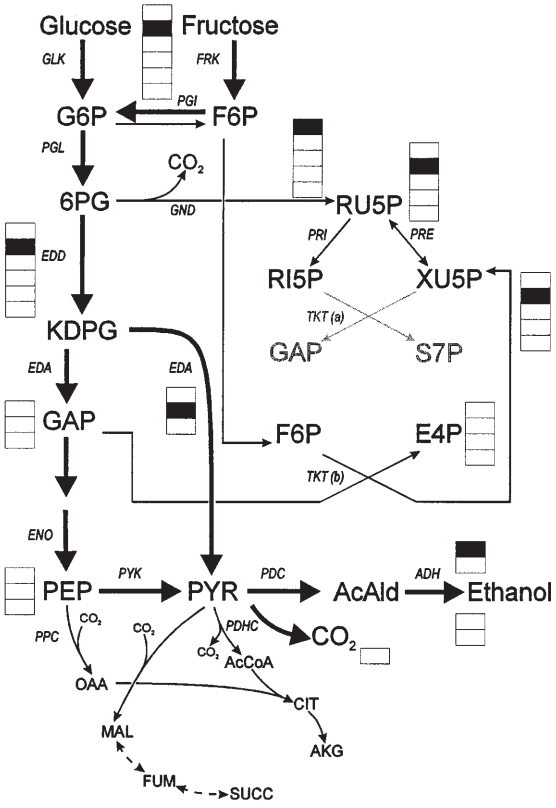

Fig. 2 Scheme of the fate of [2-^{13}C] label (*shaded box*) from glucose and fructose during metabolism in *Zymomonas mobilis*. Of each two pyruvate molecules formed from 2-keto-3-deoxy-6-phosphogluconate (*KDPG*), one is labelled in C-2, while the other is unlabelled since its carbons originate from C-4, C-5 and C-6 of KDPG. Ribose 5-phosphate is labelled in C-1 or C-2 depending on whether it is formed via 6-phosphogluconate dehydrogenase or transketolase(b), respectively (*GLK* glucokinase, *FRK* fructokinase, *PGI* phosphoglucose isomerase, *PGL* phosphogluconolactonase, *GND* 6-phosphogluconate dehydrogenase, *EDD* 6-phosphogluconate dehydratase, *EDA* 2-keto-3-deoxy-gluconate aldolase, *ENO* enolase, *PYK* pyruvate kinase, *PPC* phospho*enol*pyruvate carboxylase, *PDC* pyruvate decarboxylase, *PDHC* pyruvate dehydrogenase complex, *ADH* alcohol dehydrogenases I and II, *XI* xylose isomerase, *XK* xylulokinase, *PRE* ribulose-5-phosphate epimerase, *PRI* phosphoribose isomerase, *TKT* transketolase, *TAL* transaldolase, *G6P* glucose 6-phosphate, *F6P* fructose 6-phosphate, *6PG* 6-phosphogluconate, *GAP* glyceraldehyde-3-phosphate, *PEP* phospho*enol*pyruvate, *PYR* pyruvate, *RU5P* ribulose 5-phosphate, *RI5P* ribose 5-phosphate, *XU5P* xylulose 5-phosphate, *S7P* sedoheptulose 7-phosphate, *E4P* erythrose 4-phosphate, *AcAld* acetaldehyde, *OAA* oxaloacetate, *AcCoA* acetyl-coenzyme A, *CIT* citrate, *AKG* 2-oxoglutarate, *MAL* malate, *FUM* fumarate, and *SUCC* succinate)

Biomass composition

For a comprehensive flux analysis, the requirements of basic precursor metabolites for the synthesis of biomass must be accounted for as done, for example, by Marx et al. (1996). Combining the available data on the biomass composition of *Z. mobilis* (Swings and De Ley 1977) with those of another gram-negative organism, *E. coli* (Neidhardt et al. 1990), an overall biomass composition of *Z. mobilis* as given in Table 1 is arrived at. The protein composition of *Z. mobilis* as given in Sutter (1991) was then used to calculate from Table 1 the detailed precursor requirement for biomass synthesis as given in Table 2.

Table 1 Relative contents of the main cellular constituents of *Zymomonas mobilis* used to quantitate the precursor requirements for the synthesis of biomass in this study. Data were taken from Swings and De Ley (1977), Dawes and Large (1970) and Low and Rogers (1984), and were complemented with data from *Escherichia coli* taken from Neidhardt et al. (1990)

Component	Content (% dry weight)
Protein	60.5
RNA	19.5
DNA	2.7
Lipid	8.5
Peptidoglycan	2.5
Glycogen	2.5
Polyamines	0.3
Metabolites, ions	3.5

Results

[2-^{13}C]glucose and [2-^{13}C]fructose fermentations

Measurable fluxes and carbon balance

The fermentation volume of the [2-^{13}C]glucose fermentation was 288 ml, and the dilution rate was 0.104 h^{-1}. The overall ^{13}C enrichment in C-2 was 20.7%. The steady-state biomass concentration in the fermentor was 1.24 g dry wt./l at no residual glucose. Thus, the specific glucose uptake rate was 525 µmol · (g dry wt.)$^{-1}$ · min^{-1}, and the specific biomass yield was 0.018 g dry wt./g glucose, or 3.2 g dry wt./mol of glucose. Based on this value, the fluxes of precursors for biomass synthesis were calculated from Table 2. They are presented in Table 3. According to this analysis, only 2.0% of the total carbon was used for biomass synthesis. This is a typical figure for *Z. mobilis* (Swings and De Ley 1977). An elementary composition analysis of the cells, on the other hand, showed that carbon constituted 43.5% of the dry weight, equivalent to 1.9% of the total carbon having been used for biomass synthesis. This value compares well with the 2.0 obtained using the biomass composition data from Tables 1 and 2.

For the fructose fermentation, the data were very similar: culture volume, 300 ml; 20.7% ^{13}C label in C-2; steady-state biomass concentration, 1.37 g dry wt./l; specific fructose uptake rate, 469 µmol · (g dry wt.)$^{-1}$ · min^{-1}; specific biomass yield, 3.6 g dry wt./mol of fructose. Based on these values, the fluxes of precursors for biomass synthesis were again calculated from Table 2 and presented in Table 3 (third and fourth columns). According to this analysis, 2.2% of the total carbon was used for biomass synthesis, slightly more than for the glucose fermentation. The elementary composition analysis of the cells indicated a 49.6% carbon content of the biomass, equivalent to 2.4% of the total carbon uptake. This value again compares well with the 2.2 obtained using the biomass composition data from Tables 1 and 2.

The fermentation broth was analysed for a number of products and by-products common to *Z. mobilis*, and the results are given in Table 4. As expected, ethanol and carbon dioxide were the principal products. The main by-products were lactate and acetaldehyde in the glucose fermentation, and lactate plus glycerol in the fructose fer-

Table 2 Calculated precursor requirements for *Zymomonas mobilis* biomass synthesis, calculated from Table 1 using data on protein composition of *Z. mobilis* given in Sutter (1991). The precise source and fate of CO_2 in biomass synthesis is needed to keep track of its ^{13}C label. Origin and fate of CO_2 label: 687 μmol/g dry wt. is fixed in RNA/DNA synthesis (precursor RI5P); 181 μmol/g dry wt. is fixed in Arg synthesis (precursor AKG); 135 μmol/g dry wt. with label of PEP-C1 is freed in the synthesis of the three aromatic amino acids; and 4,325 μmol/g dry wt. with label of pyruvate-C1 is freed in the synthesis of Ile, Lys, Leu and Val (1,925 μmol/g dry wt.) and with AcCoA (2,400 μmol/g dry wt.). (*G6P* glucose 6-phosphate, *F6P* fructose 6-phosphate, *RI5P* ribose 5-phosphate, *E4P* erythrose 4-phosphate, *GAP* glyceraldehyde-3-phosphate, *PGA* phosphoglycerate, *PEP* phospho*enol*pyruvate, *PYR* pyruvate, *AcCoA* acetyl-coenzyme A, *OAA* oxaloacetate, and *AKG* 2-oxoglutarate)

Amino acid	Amount (μmol/g dry weight)	Precursor stoichiometry (mol/mol amino acid)												
		G6P	F6P	RI5P	E4P	GAP	PGA	PEP	PYR	AcCoA	OAA	AKG	CO_2	NADPH
Ala	1088								1				1	8
Arg	181											1	1	4
Asx	478										1			1
Cys	20						1							5
Glx	343											1		1
Gly	920						1							1
His	82			1										1
Ile	369								1		1		–1	5
Leu	369								2	1			–2	2
Lys	249								1		1		–1	4
Met	81										1			8
Phe	11				1			2					–1	2
Pro	210											1		3
Ser	202						1							1
Thr	224										1			3
Trp	54			1	1			1					–1	2
Tyr	70				1			2					–1	2
Val	569								2				–1	2

Polymer	Precursor amount (μmol/g dry weight)												
	G6P	F6P	RI5P	E4P	GAP	PGA	PEP	PYR	AcCoA	OAA	AKG	CO_2	NADPH
Protein	0	0	136	135	0	1142	216	3582	369	1401	734	–	–
RNA			600			350				250		600	406
DNA			87			44				44		87	174
Lipids					120	120			1976			–1976	3615
Peptidoglycan		55					28	83	55	28	28	–55	193
Glycogen	154												0
C1-Units						49							49
Polyamines											59		180
Total	154	55	823	135	120	1705	244	3665	2400	1723	821	–	–

Table 3 Precursor requirement fluxes for the three fermentations. The fluxes were normalized to the total carbon uptake (% C) or the molar uptake rate (% rate) of the substrate, respectively (*G6P* glucose 6-phosphate, *F6P* fructose 6-phosphate, *RI5P* ribose 5-phosphate, *E4P* erythrose 4-phosphate, *S7P* sedoheptulose 7-phosphate, *GAP* glyceraldehyde-3-phosphate, *PGA* phosphoglycerate, *PEP* phospho*enol*pyruvate, *PYR* pyruvate, *AcCoA* acetyl-coenzyme A, *OAA* oxaloacetate, and *AKG* 2-oxoglutarate)

Precursor	Relative flux					
	Glucose		Fructose		Xylose	
	% C	% Rate	% C	% Rate	% C	% Rate
G6P	0.049	0.049	0.055	0.055	0.049	0.041
F6P	0.017	0.017	0.019	0.019	0.018	0.015
RI5P	0.218	0.262	0.243	0.292	0.219	0.219
E4P	0.029	0.043	0.032	0.048	0.029	0.036
S7P	0.009	0.008	0.010	0.009	0.008	0.006
GAP	0.019	0.038	0.021	0.043	0.019	0.032
PGA+PEP	0.310	0.620	0.346	0.692	0.311	0.518
PYR+AcCoA	0.965	1.929	1.077	2.153	1.292	1.613
OAA	0.365	0.548	0.408	0.612	0.367	0.459
AKG	0.218	0.261	0.242	0.291	0.217	0.218
CO_2	–0.190	1.142	–0.213	1.275	–0.192	0.955
Total	2.01	–	2.24	–	2.34	–

Table 4 Biomass, substrate and product concentrations measured in the fermentation broths of the three fermentations. Values in parentheses represent the substrate concentrations in the medium. The typical measurement imprecision was 10% for biomass and for products other than CO_2 and ethanol (*ND* no gas analysis for ethanol was performed)

[a] The concentrations measured in the fermentor efflux gas were converted to equivalent concentrations in the liquid phase resulting in the same efflux at the given fermentor dilution rate

[b] Ethanol (gas) and CO_2 showed more variation than during glucose and fructose fermentation

Compound	Concentration in the fermentation broth (mM)		
	Glucose (388.8 mM)	Fructose (385 mM)	Xylose (466 mM)
Residual substrate	0.1	3.5	28
Ethanol	632 ± 17	692 ± 19	286 ± 8
Ethanol (gas)	ND	111 ± 3	301 ± 90[b]
CO_2[a]	506 ± 298	571 ± 30	483 ± 90[b]
Sorbitol	0.8	0.1	0.0
Xylitol	0.0	0.0	19.0
Xylulose	0.0	0.0	3.8
Glycerol	2.2	5.7	5.6
Lactate	5.5	9.3	0.7
Acetoine	2.5	0.0	0.0
Acetate	2.1	3.0	8.9
Acetaldehyde	4.6	2.6	1.7
Dihydroxyacetone	0.0	3.9	0.0
Other C-3 compounds	0.0	0.0	4.4

Table 5 Carbon balances for the three chemostat cultures. Citrate taken up from the medium was negligible and therefore was not taken into account. Typical measurement imprecision was 10% for biomass and for products other than CO_2 and ethanol

[a] No gas analysis for ethanol was performed in this case

Compound	% of total carbon		
	Glucose	Fructose	Xylose
Residual substrate	0.0	0.9	6.0
Biomass	1.9	2.4	1.9
Ethanol	54.2 ± 1.5	68.9 ± 1.9	50.3 ± 8.4
CO_2	22 ± 13	24.5 ± 1.3	20.7 ± 3.9
Xylitol	0.0	0.0	4.1
Other by-products	2.2	2.9	3.1
Total	80 ± 15[a]	99.6 ± 3.9	86 ± 14

mentation. Concentrations of lactate, glycerol, acetate and dihydroxyacetone were significantly higher in the fructose fermentation (2.7% C vs 1.2%), while those of sorbitol, acetoine and acetaldehyde were lower (0.3% C vs 0.9%). Table 4 also shows the value for carbon dioxide, of which the relative volumetric content in the fermentor waste gas (20 l argon/h) was 1.7 ± 1% (measured with an analyser calibrated for the 0–100% range) for the glucose experiment and 1.8 ± 0.1% for the fructose experiment. The normal molar volume of 22.4 l/mol of gas was then used to convert that value to moles of CO_2 released per hour from the cultures.

The data from Table 4 were converted to yield the carbon balance of the cultures given in Table 5. For the glucose fermentation, biomass and by-products, each accounted for 2%, so the remaining 96% must have been metabolized to ethanol and CO_2 in approximately equimolar amounts. Thus, 32% of carbon is expected in carbon dioxide, and 64% in ethanol. While the CO_2 value lies in the large measurement error interval, the measured ethanol amount definitely is too low, which must be due to evaporation from the culture that was not accounted for. Therefore, ethanol analysis of the fermentor waste gas was done for the ensuing fructose and xylose fermentations. The data for the fructose fermentation (Tables 4 and 5) then showed a better carbon balance, with the ethanol content slightly more than the theoretically predicted 62.6%, and the carbon dioxide content lower than the theoretically predicted 31.3%.

Measured ^{13}C enrichments

The amino acids and nucleotides obtained from biomass hydrolysis were subjected to NMR analysis as described in Materials and methods to quantitate the ^{13}C label distribution in the precursors from the central metabolism. The results for the glucose and fructose experiments are given in Tables 6 and 7. The results for the two substrates are identical within experimental error, indicating virtually identical flux distributions in the two cases. Except for ribose 5-phosphate, the measured ^{13}C enrichments are in perfect agreement with the labelling patterns expected for *Z. mobilis* that are depicted in Fig. 2: no label in PEP, which derives from unlabelled carbons 4, 5 and 6 of the substrate, and approximately half the original substrate C-2 label of 20.7% found in pyruvate C-2, i.e. 10.2%. The fact that all carbons of oxaloacetate and carbons 1, 2 and 3 of 2-oxoglutarate were unlabelled confirms previous investigations, from which it was concluded that *Z. mobilis* does not have a functional citric acid cycle (Dawes et al. 1970; Bringer-Meyer and Sahm 1993).

The fact that 20% ^{13}C enrichment was found in C-2 of ribose 5-phosphate and only 1.3% in C-1 (Table 6) was somewhat surprising since it implies that the relative amounts of ribose 5-phosphate formed via the nonoxidative pentose phosphate pathway as opposed to other reactions during glucose fermentation are (19 ± 2)/(0.2 ± 0.2),

Table 6 ^{13}C enrichments in precursor metabolites derived from the experiment with [2-^{13}C]glucose as substrate. The input label was 20.7% in C-2, and 1.1% (i.e. natural abundance) in all other carbons. *Values in italics* are the corresponding values as predicted from the best estimate for the flux distribution. The data were derived from the NMR-measured amino acids and nucleotides isolated from the hydrolysed biomass as follows: PGA from Gly and Ser; OAA from Asp and Thr; AKG from Glu and Arg; PYR from Ala, Leu and Val; PEP from Phe; E4P from Phe; RI5P from cytidine (*PGA* phosphoglycerate, *OAA* oxaloacetate, *AKG* 2-oxoglutarate, *PYR* pyruvate, *PEP* phospho*enol*pyruvate, *E4P* erythrose 4-phosphate, *RI5P* ribose 5-phosphate, and *nd* not determined)

Metabolite	Relative ^{13}C enrichment in carbon number				
	1	2	3	4	5
Ethanol	10.6 ± 0.2 *11.0*	1.05 ± 0.07 *1.1*			
PGA	1.20 ± 0.14 *1.1*	1.5 ± 0.5 *1.1*	0.1 ± 1 *1.1*		
OAA	1.2 ± 0.4 *1.1*	1.1 ± 0.3 *1.1*	1.21 ± 0.07 *1.1*	0.94 ± 0.06 *1.1*	
AKG	0.9 ± 0.3 *1.1*	1.1 ± 0.3 *1.1*	1.0 ± 0.4 *1.1*	0.9 ± 0.3 *1.1*	10.7 ± 0.3 *11.0*
PYR	1.1 ± 0.1 *1.1*	10.2 ± 0.3 *11.0*	1.07 ± 0.05 *1.1*		
PEP	nd *1.1*	1.0 ± 0.3 *1.1*	1.4 ± 0.5 *1.1*		
E4P	1.1 ± 0.1 *1.1*	1.1 ± 0.1 *1.1*	1.1 ± 0.1 *1.1*	1.1 ± 0.1 *1.1*	
RI5P	1.3 ± 0.2 *1.3*	20 ± 2 *20.5*	nd *1.1*	nd *1.1*	nd *1.1*

Table 7 ^{13}C enrichments in precursor metabolites derived from the experiment with [2-^{13}C]fructose as substrate. The input label was 20.7% in C-2, and 1.1% (i.e. natural abundance) in all other carbons. *Values in italics* are the corresponding values as predicted from the best estimate for the flux distribution. The data were derived from the NMR-measured amino acids and nucleotides isolated from the biomass hydrolysate as follows: PGA from Gly and Ser; OAA from Asp and Thr; AKG from Glu and Arg; PYR from Ala, Leu and Val; PEP from Phe; E4P from Phe; RI5P from guanosine (*PGA* phosphoglycerate, *OAA* oxaloacetate, *AKG* 2-oxoglutarate, *PYR* pyruvate, *PEP* phospho*enol*pyruvate, *E4P* erythrose 4-phosphate, and *RI5P* ribose 5-phosphate)

Metabolite	Relative ^{13}C enrichment in carbon number				
	1	2	3	4	5
Ethanol	10.45 ± 0.2 *11.1*	1.1 ± 0.1 *1.1*			
PGA	0.8 ± 0.4 *1.1*	1.1 ± 0.1 *1.1*	0.7 ± 0.5 *1.1*		
OAA	1.1 ± 0.2 *1.1*	1.1 ± 0.2 *1.1*	0.9 ± 0.4 *1.1*	1.2 ± 0.1 *1.1*	
AKG	nd *1.1*	1.1 ± 0.5 *1.1*	1.2 ± 0.4 *1.1*	0.7 ± 0.5 *1.1*	10.7 ± 0.3 *11.1*
PYR	1.4 ± 0.5 *1.1*	10.2 ± 0.4 *11.1*	1.0 ± 0.2 *1.1*		
PEP	1.1 ± 0.2 *1.1*	1.0 ± 0.3 *1.1*	0.9 ± 0.3 *1.1*		
E4P	1.1 ± 0.2 *1.1*	1.1 ± 0.2 *1.1*	1.1 ± 0.2 *1.1*	1.1 ± 0.2 *1.1*	
RI5P	1.6 ± 0.3 *1.5*	20.4 ± 0.4 *20.3*	1.4 ± 0.4 *1.1*	1.2 ± 0.4 *1.1*	1.0 ± 0.2 *1.1*

i.e. at least 42 but likely 100 or more. A similar ratio was found for the fructose fermentation.

Flux distributions

The results of the flux estimation for the two cultures is presented in Table 9. The ^{13}C enrichments in precursor metabolites predicted from these flux distributions are given in Tables 6 and 7 for comparison with the measured data. The agreement is excellent, with average deviations between measured and predicted data, normalized to the measurement error, only 1.0 and 0.8 for the glucose and fructose experiments, respectively. The results clearly show that almost all of the sugar is very rapidly metabolized over the Entner-Doudoroff pathway with very little drain-offs to by-products and cell mass synthesis. Only negligible net fluxes are carried by the transketolase(a), transketolase(b), 6-phosphogluconate dehydrogenase, ribulose-5-phosphate epimerase and ribose-5-phosphate isomerase reactions, but the flux analysis predicts large [transketolase(a) and ribulose-5-phosphate epimerase] to excessive [ribose-5-phosphate isomerase and transketolase(b)] exchange fluxes in the nonoxidative pentose phosphate pathway during the glucose fermentation. The flux estimation result also predicts a rapid equilibration of the glucose 6-phosphate and fructose 6-phosphate pools via the reversible phosphoglucose isomerase reaction. All these exchange fluxes, except for transketolase(b), were no longer indentifiable from the data from the fructose experiment. However, in the context of the model used, the strong labelling of ribose 5-phosphate C-2 could only be due to the presence of significant reversibility in the transketolase(b) reaction and of equilibration of the pentose 5-phosphate pools, which were therefore merged into a single pool in order to allow duly for quantitation of the exchange flux in the transketolase(b) reaction. Obviously, the flux distributions thus determined reveal no clues to the differences between glucose and fructose metabolism.

[1-^{13}C]xylose fermentation

Measurable fluxes and carbon balance

The fermentation data for the [1-^{13}C]xylose fermentation were as follows: culture volume, 300 ml; 19.7% ^{13}C label in C-1; steady-state biomass concentration, 1.16 g dry wt./l; specific xylose uptake rate, 108 μmol · (g dry wt.)$^{-1}$ · min^{-1}; and specific biomass yield, 2.7 g dry wt./mol of xylose. Based on these values, the fluxes of precursors for biomass synthesis were calculated from Table 2 and pre-

sented in Table 3 (fifth and sixth columns). According to this analysis, 2.3% of the total carbon was used for biomass synthesis, slightly more than for the fructose fermentation. The elementary composition analysis of the cells indicated a 46.2% carbon content of the biomass, equivalent to 1.9% of the total carbon uptake. This value is 20% lower than the one obtained using the biomass composition data from Tables 1 and 2, possibly reflecting a somewhat altered biomass composition as compared to growth on glucose and fructose.

The amount of carbon used for the synthesis of by-products, 7.2% (Table 5), was more than threefold increased as compared to the glucose fermentation. The by-product spectrum (Table 4) was different from that of the glucose and fructose fermentations, the principal components now being xylose-derived xylitol and the intermediate xylulose (5.2 carbon %). More acetate was produced, but much less lactate. Signals from several yet unidentified by-products could be observed in the proton-NMR spectrum of the culture supernatant. These were estimated to account for 1.0% in the carbon balance. It is an interesting fact that apart from the xylose-derived by-products, the amount of carbon used for by-product synthesis was 3.0%, which is almost identical to the value observed for the fructose fermentation. This signifies that on the whole, *Z. mobilis* seemed only little affected by the change from C-6 substrates to a C-5 substrate, i.e. the introduction of the heterologous genes did not lead to a disturbed redox balance in the cell. The most striking difference was in the substrate uptake rate, which was almost fivefold lower for xylose than for glucose. Also, considerable amounts of residual substrate were found in the xylose fermentation.

Residual substrate, biomass and by-products accounted for 15.1% of the carbon (Table 5). Theoretically, the remaining 84.9% should be retrieved in ethanol (56.6%) and carbon dioxide (28.3%). While the ethanol measurement was in accordance with this prediction – within experimental error –, the CO_2 measurement was somewhat lower than predicted. Since this was the case for all three fermentations, the carbon dioxide measurement may have been biased.

Measured ^{13}C enrichments

The NMR results for the xylose experiment are given in Table 8. Disregarding the oxidative pentose phosphate pathway and biosynthetic reactions, pathway stoichiometry predicts that from three molecules of xylose, three molecules of glyceraldehyde-3-phosphate and two molecules of pyruvate will result. After inspection of the labelling patterns (Fig. 3) and assuming a 20% ^{13}C enrichment in xylose C-1 and a 1.1% enrichment (i.e. natural abundance) in all other carbons, the expected labellings are: 20% in ribose 5-phosphate C-1, 8.6% in pyruvate C-1, 4.8% in pyruvate C-3 and ethanol C-2, and 8.6% in CO_2. The CO_2 label is also expected in oxaloacetate C-4 and in 2-oxoglutarate C-1. Only natural-abundance ^{13}C is expected in PEP. Comparing this with the experimentally determined values (Table 8), it is apparent that while this basic pattern is indeed observed, all enrichments are lower than predicted, and several carbons bear enrichments that were not predicted from the simple stoichiometric model (ethanol C-1, pyruvate C-2, erythrose 4-phosphate C-1, and ribose 5-phosphate C-2 and C-5. Thus, significant label scrambling occurred. This observation is typical for cases where the transaldolase and/or transketolase reactions of the pentose phosphate pathway show a significant degree of reversibility (Marx et al. 1996; Wiechert and De Graaf 1997; Wiechert et al. 1997). For instance, a reversible transketolase(b) reaction in Fig. 3 would transfer label from fructose 6-phosphate C-3 [resulting from the transketolase(a) and transaldolase reactions] to erythrose 4-phosphate C-1. Upon subsequent reversible operation of transaldolase and transketolase(a), this label would reach ribose 5-phosphate C-2. However, also 6-phosphogluconate dehydrogenase activity would transfer label from 6-phosphogluconate C-3 to ribose 5-phosphate C-2 in a single step.

Table 8 ^{13}C enrichments in precursor metabolites resulting from the experiment with [1-^{13}C]xylose as substrate. The input label was 19.7% in C-1, and 1.1% (i.e. natural abundance) in all other carbons. *Values in italics* are the corresponding values as predicted from the best estimate for the flux distribution. The data were derived from the NMR-measured amino acids and nucleotides isolated from the hydrolysed biomass as follows: PGA from Gly and Ser; OAA from Asp and Thr; AKG from Glu and Arg; PYR from Ala, Leu and Val; PEP from Phe; E4P from Phe; and RI5P from guanosine. The ^{13}C enrichment in CO_2 was determined by infrared spectroscopy (Marx et al. 1999) (*PGA* phosphoglycerate, *OAA* oxaloacetate, *AKG* 2-oxoglutarate, *PYR* pyruvate, *PEP* phospho*enol*pyruvate, *E4P* erythrose 4-phosphate, *RI5P* ribose 5-phosphate and *nd* not determined)

Metabolite	Relative ^{13}C enrichment in carbon number				
	1	2	3	4	5
Ethanol	3.8 ± 0.4 *1.5*	4.5 ± 0.2 *4.5*			
PGA	nd *1.1*	nd *1.1*	nd *1.1*		
OAA	1.3 ± 0.2 *1.1*	0.5 ± 0.7 *1.1*	0.5 ± 0.7 *1.1*	8.3 ± 0.4 *8.3*	
AKG	8.2 ± 0.3 *7.9*	0.3 ± 0.9 *1.1*	1.5 ± 0.2 *1.1*	3.9 ± 0.3 *4.3*	nd *1.5*
PYR	7.0 ± 0.5 *7.5*	3.0 ± 1.5 *1.5*	4.5 ± 0.3 *4.5*		
PEP	0.7 ± 0.6 *1.1*	1.1 ± 0.5 *1.1*	0.8 ± 0.5 *1.1*		
E4P	4.3 ± 0.4 *4.3*	1.1 ± 1 *1.1*	1.1 ± 1 *1.1*	1.1 ± 0.2 *1.1*	
RI5P	19.1 ± 0.6 *17.6*	2.7 ± 1.3 *2.2*	1.1 ± 0.5 *1.1*	1.1 ± 0.5 *1.1*	2.4 ± 1.0 *1.1*
CO_2	8.1 ± 0.5 *8.3*				

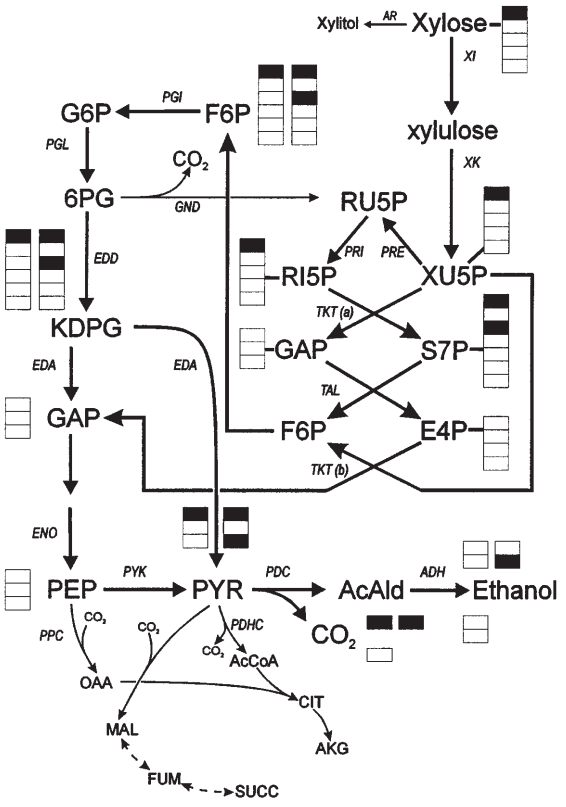

Fig. 3 Scheme of the fate of [1-^{13}C] label (*shaded box*) from xylose during metabolism in *Zymomonas mobilis* CP4/pZY228/pZY557*tal*. Basic stoichiometry predicts that two molecules of fructose 6-phosphate and one molecule of glyceraldehyde-3-phosphate are formed from three molecules of xylose. One fructose 6-phosphate is labelled in C-1, the other in both C-1 and C-3. This leads to four molecules of pyruvate: two unlabelled, one labelled in C-1, and one double-labelled in C-1 and C-3. The glyceraldehyde-3-phosphate resulting from the transketolase(b) reaction is unlabelled and gives rise to unlabelled pyruvate. Following this basic scheme, ribose 5-phosphate will only be labelled in C-1, and no label will be present in erythrose 4-phosphate. However, [2-^{13}C]ribose-5-phosphate may result from [1,3-$^{13}C_2$]6-phosphogluconate metabolized via 6-phosphogluconate dehydrogenase, and [1-^{13}C]erythrose-4-phosphate may result from [1,3-$^{13}C_2$]fructose-6-phosphate via reverse operation of transketolase(b) (*AR* aldoreductase, *PGL* phosphogluconolactonase, *GND* 6-phosphogluconate dehydrogenase, *EDD* 6-phosphogluconate dehydratase, *EDA* 2-keto-3-deoxy-gluconate aldolase, *ENO* enolase, *PYK* pyruvate kinase, *PPC* phospho*enol*pyruvate carboxylase, *PDC* pyruvate decarboxylase, *PDHC* pyruvate dehydrogenase complex, *ADH* alcohol dehydrogenases I and II, *XI* xylose isomerase, *XK* xylulokinase, *PRE* ribulose-5-phosphate epimerase, *PRI* phosphoribose isomerase, *TKT* transketolase, *TAL* transaldolase, *G6P* glucose 6-phosphate, *F6P* fructose 6-phosphate, *6PG* 6-phosphogluconate, *KDPG* 2-keto-3-deoxy-6-phosphogluconate, *GAP* glyceraldehyde-3-phosphate, *PEP* phospho*enol*pyruvate, *PYR* pyruvate, *RU5P* ribulose 5-phosphate, *RI5P* ribose 5-phosphate, *XU5P* xylulose 5-phosphate, *S7P* sedoheptulose 7-phosphate, *E4P* erythrose 4-phosphate, *AcAld* acetaldehyde, *OAA* oxaloacetate, *AcCoA* acetyl-coenzyme A, *CIT* citrate, *AKG* 2-oxoglutarate, *MAL* malate, *FUM* fumarate, and *SUCC* succinate)

Flux distribution

The subsequent flux estimation solved these questions. It indicated (Table 9) that almost one-fifth, i.e. 18%, of the total fructose 6-phosphate formed in the transaldolase and transketolase(b) reactions was recycled over the oxidative pentose phosphate pathway (6-phosphogluconate dehydrogenase) to ribulose 5-phosphate (Table 9), thereby causing the elevated enrichment of ribose 5-phosphate C-2. Indeed, one exchange flux could be identified from the data, namely transketolase(b), in which the total forward flux was 49.8 and the simultaneous reverse flux was 14. The estimated relative standard deviations for this exchange flux and for the 6-phosphogluconate dehydrogenase flux were 23%.

The ^{13}C enrichments in precursor metabolites predicted from the flux distribution are given in Table 8 for comparison with the measured data. The average deviation, normalized to the measurement error, between measured and predicted data was 1.5 for this fit. The discrepancy between the experimental and predicted values for ethanol C-1 alone contributed 50% to the total sum-of-squares error function, suggesting a measurement error.

Enzyme activities

The enzyme activities of xylose isomerase, xylulokinase, transaldolase, transketolase, and phosphoglucose isomerase determined from cells cultivated in independent batch fermentations using the same xylose medium as for the continuous culture are given in Table 10. Obviously, the specific activities of all these enzymes vary very little during the fermentation. Except for xylulokinase, the theoretical flux capacities derived from these activities are as large as 785 (phosphoglucose isomerase) to 1,400 μmol · (g dry wt.)$^{-1}$ · min^{-1} (other enzymes), which would be perfectly adequate to sustain the glycolytic rates observed during glucose or fructose metabolism (Table 9) . The specific activity of xylulokinase, however, suggests a maximum flux capacity of 91 μmol · (g dry wt.)$^{-1}$ · min^{-1} for this enzyme, which is close to the 102 μmol · (g dry wt.)$^{-1}$ · min^{-1} determined from the flux estimation (Table 9). Therefore, our data suggest a rate-limiting step in *Z. mobilis* CP4/pZY228/pZY557*tal* at the level of xylulokinase. The occurrence of xylulose in the culture underlines this.

Metabolite pool size investigations using ^{31}P-NMR spectroscopy

The flux analysis results obtained for glucose and fructose as substrates were almost identical (Table 9). Nevertheless, the by-product spectrum observed with the two sugars differed considerably (Table 4). A puzzling fact is that, except for sorbitol, which represents a very minor by-product, all these by-products derive from precursors at the level of glyceraldehyde-3-phosphate or even further down the Entner-Doudoroff pathway, i.e. from sections of

Table 9 Intracellular flux distributions for the three fermentations as determined by nonlinear least-squares fitting of the flux model (Fig. 1) to the NMR and fermentation data. All fluxes are expressed on a molar basis as a percentage of the specific substrate uptake rate. *Values in parentheses* represent the specific substrate uptake rates (*NI* presumably present but not identifiable from the data, *GLK* glucokinase, *FRK* fructokinase, *XI* xylose isomerase, *XK* xylulokinase, *PGI* phosphoglucose isomerase, *PGL* phosphogluconolactonase, *EDD* 6-phosphogluconate dehydratase, *EDA* 2-keto-3-deoxy-gluconate aldolase, *ENO* enolase, *PYK* pyruvate kinase, *PDC* pyruvate decarboxylase, *ADH* alcohol dehydrogenases I and II, *PRE* ribulose-5-phosphate epimerase, *PRI* phosphoribose isomerase, *TKT* transketolase, *TAL* transaldolase, *GND* 6-phosphogluconate dehydrogenase, *PPC* phospho*enol*pyruvate carboxylase, and *PDHC* pyruvate dehydrogenase complex)

Flux name	Flux value (%)					
	Glucose [uptake 525 μmol (g dry weight)$^{-1}$ min^{-1}]		Fructose [uptake 469 μmol (g dry weight)$^{-1}$ min^{-1}]		Xylose [uptake 108 μmol (g dry weight)$^{-1}$ min^{-1}]	
	Net	Exchange	Net	Exchange	Net	Exchange
GLK	100.0	–[1]	–	–	–	–
FRK	–	–	100.0	–	–	–
XI	–	–	–	–	94.8[2]	–
XK	–	–	–	–	94.8	–
PGI	0.2	99	99.9	NI	71.6	NI
PGL	99.8	–	99.9	–	71.6	–
EDD	99.4	–	99.6	–	58.6	–
EDA	99.4	–	99.6	–	58.6	–
ENO	98.8	–	97.1	–	93.1	–
PYK	97.4	–	95.5	–	92.4	–
PDC	192.6	–	190.3	–	149.8	–
ADH	190.2	–	188.8	–	145.4	–
PRE[3]	0.1	20.0	0.1	NI	23.1	NI
PRI[3]	0.3	230	0.3	NI	36.1	NI
TKT(a)	0.0	4.9	0.0	NI	35.8	NI
TAL	–	–	–	–	35.8	NI
TKT(b)	0.0	142	0.0	13	35.8	14
GND	0.3	–	0.3	–	13.0	–
PPC	0.8	–	0.9	–	0.7	–
PDHC	1.0	–	1.2	–	0.9	–

[1] "–" signifies that the corresponding flux was not included in the model

[2] The remaining 5.2% was metabolized to the by-product xylitol

[3] The ribulose 5-phosphate, xylulose 5-phosphate and ribose 5-phosphate pools were merged into a single pentose phosphate pool for the modeling of the fructose and xylose fermentations. This is equivalent to setting the ribulose-5-phosphate epimerase and ribose-5-phosphate isomerase exchange fluxes to an infinitely high value

the metabolism that are common to both fructose and glucose metabolism. Therefore, ^{31}P-NMR spectroscopy in vivo and on cell-free chloroform extracts was performed to investigate intracellular metabolite levels.

Representative in vivo ^{31}P-NMR spectra obtained using the membrane cyclone bioreactor are shown in Fig. 4 A and B. Table 11 shows the intracellular pool sizes calculated from the spectra. These results reveal a very significant, overall difference between intracellular energetic pools during glucose and fructose fermentation. NDP, NTP, UDP-sugar and intracellular inorganic phosphate concentrations were all approximately twofold lower during fructose metabolism. Total NAD(P)(H) pools were identical, but the glucose-fermenting cells showed a higher concentration of cyclic pyrophosphate (previously identified as 2-methylbutane-1,2,3,4-tetrahydroxy-2,4-cyclopyrophosphate; G. Schmitz, unpublished work) and a derivative of it, as well as of polyphosphate, which was absent from fructose-growing cells. Most striking, the total sugar phosphate concentration during fructose metabolism was fivefold higher than during glucose fermentation. Since the various different individual sugar phosphates could not be identified in the in vivo spectra, ^{31}P-NMR measurements of cell-free chloroform extracts from the two cultures were performed. Two representative spectra are shown in Fig. 5 A and B. While consistency checks indicated that almost 50% of the intracellular metabolites were found in the 60% methanol supernatant, the spectra clearly reflect a large difference in composition of the sugar phosphate pools between the two experiments. Due to the extreme sensitivity of the sugar phosphate resonance positions towards changes in the sample composition, only a few metabolites could be unambiguously identified. Thus, the largest resonance in both spectra, which was twofold higher for the fructose-grown cells, was 3-phosphoglycerate. Resonances that could be tentatively assigned to fructose 6-phosphate, ribose 5-phosphate, sedoheptulose 7-phosphate and dihydroxyacetone phosphate were also several-fold more intense for the fructose-grown cells. The peaks from glu-

Table 10 Specific activities of xylose isomerase(*XI*), xylulokinase (*XK*), transaldolase (*TAL*), transketolase (*TKT*), and phosphoglucose isomerase (*PGI*) determined in *Zymomonas mobilis* CP4/pZY228/pZY557*tal* cells taken at various time points during the fermentation of xylose from independent batch fermentations using the same medium as for the continuous culture

Time (h)	Specific activity (U/mg protein)				
	TAL	*TKT*	*XI*	*XK*	*PGI*
29	2.7 ± 0.1	2.5 ± 0.1	2.1 ± 0.1	0.15 ± 0.02	1.2 ± 0.2
48	2.6 ± 0.1	2.5 ± 0.1	2.3 ± 0.1	0.15 ± 0.02	1.3 ± 0.1
52	2.3 ± 0.1	3.0 ± 0.1	2.2 ± 0.1	0.14 ± 0.03	1.4 ± 0.1
72	2.3 ± 0.1	2.8 ± 0.1	1.9 ± 0.1	0.15 ± 0.03	1.3 ± 0.1

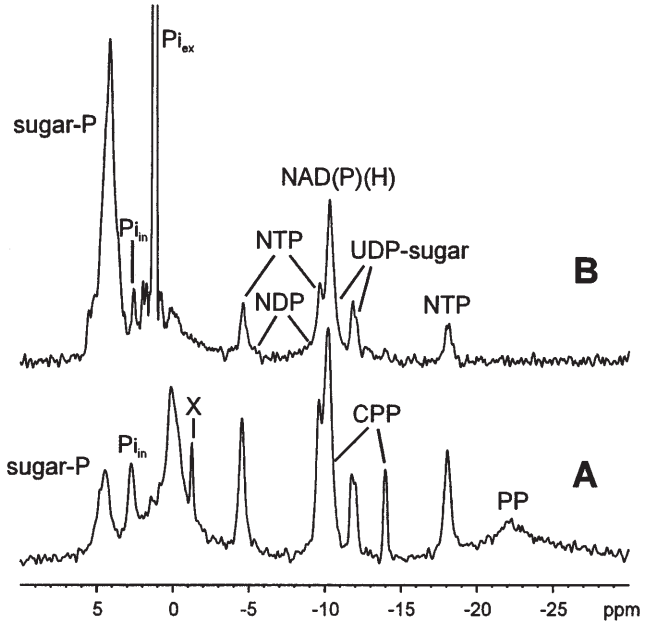

Fig. 4 In vivo ^{31}P-NMR spectra of high-cell-density cultures of *Zymomonas mobilis* fermenting **A** glucose or **B** fructose in the membrane cyclone bioreactor [*sugar-P* total sugar phosphates, Pi_{in} intracellular inorganic phosphate, Pi_{ex} extracellular phosphate, *NDP* nucleoside diphosphates, *NTP* nucleoside triphosphates, *NAD* nicotine adenine dinucleotide, *UDP-sugar* uridine diphosphate sugar, *CPP* cyclic pyrophosphate, *X* unknown derivative of CPP, *PP* polyphosphate; assignments, Hartbrich et al. (1996)]

cose 6-phosphate and 6-phosphogluconate were not significantly different between the spectra.

Discussion

The flux distributions during [2-^{13}C]glucose and [2-^{13}C]fructose metabolism determined in this study were virtually identical, with ethanol yields and by-product spectra in accordance with the literature (Swings and De Ley 1977; Rogers et al. 1982; Viikari and Korhola 1986; Viikari 1988). While the overall fermentation carbon balances (Table 4) did not provide new insights into *Z. mobilis* metabolism, the flux analysis indicated that ribose 5-phosphate was primarily synthesized via the reversible action of transketolase since no other reaction producing [2-^{13}C]ribose-5-phosphate is present in the metabolic model used. A previous study also concluded that D-ribose derivatives in *Z. mobilis* solely arise from the nonoxidative pentose phosphate pathway (Rohmer et al. 1989). Although transketolase is present in wild-type *Z. mobilis* (Feldmann et al. 1992 a), the reported activity of 2 mU/mg

Table 11 Fermentation data and concentrations of intracellular phosphorylated metabolites during high-cell-density growth of *Zymomonas mobilis* CP4 on glucose and fructose. Cytoplasmic pool sizes were determined from the in vivo ^{31}P-NMR spectra (Fig. 4 A, B)

	Glucose fermentation	Fructose fermentation
Cell dry mass	15.3 g dry weight/l	13.7 g dry weight/l
Residual substrate	17.2 g/l	23.7 g/l
Ethanol	56.8 g/l	47.2 g/l
CO_2	11.4 l/(l · h)	12.2 l/(l · h)
Extracellular phosphate	0.2 mM	1.8 mM
Intracellular phosphate	0.5 mM	0.2 mM
Total sugar phosphates	1.8 mM	9.5 mM
NDP	0.2 mM	0.1 mM
NTP	1.9 mM	0.9 mM
UDP-sugar	1.1 mM	0.4 mM
NAD(P)(H)	4.8 mM	4.5 mM
CPP	0.8 mM	0.2 mM
Phosphate in polyphosphate	6 mM	0 mM

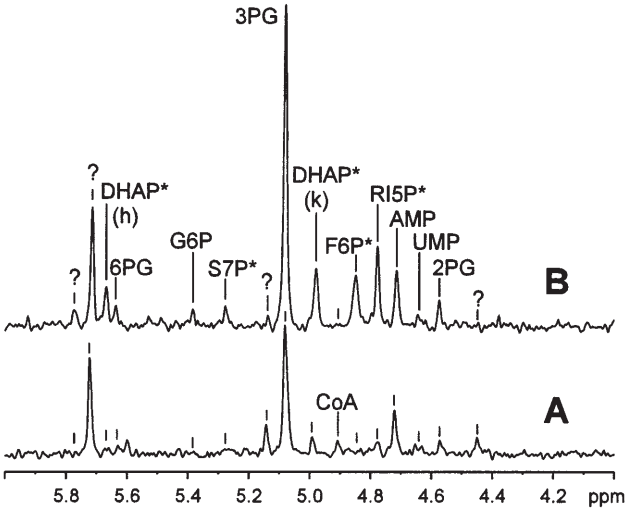

Fig. 5 ^{31}P-NMR spectra of chloroform extracts taken from high-cell-density cultures of *Zymomonas mobilis* fermenting **A** glucose or **B** fructose in the membrane cyclone bioreactor. Only the sugar phosphate region of the spectra is shown [*DHAP* dihydroxyacetone phosphate, *(h)* hydrate, *(k)* keto, *6PG* 6-phosphogluconate, *G6P* glucose 6-phosphate, *S7P* sedoheptulose 7-phosphate, *3PG* 3-phosphoglycerate, *F6P* fructose 6-phosphate, *CoA* coenzyme A, *RI5P* ribose 5-phosphate, *AMP* adenosine monophosphate, *UMP* uridine monophosphate, and *2PG* 2-phosphoglycerate; assignments, Strohhäcker et al. (1993) and J. Strohhäcker and A. A. De Graaf (unpublished work); *tentative assignments; ?unidentified peaks]

protein is far too low to explain the ^{13}C labelling pattern of ribose 5-phosphate found in this study, which would require 1.2 U/mg protein transketolase activity (Table 9) and therefore must be considered unrealistic. The latter value, however, was predicted under the model assumption that a net synthesis of ribose 5-phosphate must be primarily due to activity of 6-phosphogluconate dehydrogenase, since otherwise erythrose 4-phosphate would accumulate for which no apparent consuming reaction is present in *Z. mobilis* besides the minor amounts needed in the synthesis of the aromatic amino acids (Fig. 2). There are basically two explanations possible:

1. In *Z. mobilis*, an alternative biosynthetic pathway for synthesis of [2-^{13}C]ribose-5-phosphate exists.

2. An alternative erythrose-4-phosphate-consuming pathway other than that used for the common biosynthetic purposes is present in *Z. mobilis*. This would allow [2-^{13}C]ribose-5-phosphate to be synthesized by transketolase (rather than via 6-phosphogluconate dehydrogenase) while the concomitantly produced erythrose 4-phosphate would be consumed in the postulated reaction. This reaction would require only 1.9 mU/mg protein of enzyme activity.

The ^{13}C-based flux analyses also provided first evidence for the reversible operation of phosphoglucose isomerase, ribose-5-phosphate isomerase and ribulose-5-phosphate epimerase in vivo in *Z. mobilis* during glucose and fructose metabolism.

Whereas the [2-^{13}C]glucose and [2-^{13}C]fructose experiments generated no clues as to what might be the cause of the different by-product spectra for the two substrates, the ^{31}P-NMR experiments revealed a global difference between the intracellular phosphorylated pool size patterns in both cases. To the authors' best knowledge, no comparative data on this subject have been published thus far. From the ^{31}P-NMR results, we hypothesize that during fructose fermentation, the fructose 6-phosphate pool is much higher than during glucose catabolism (as one indeed would expect), and that this is the primary cause of a decreased growth yield and an increased by-product formation in fructose-fermenting *Z. mobilis*. This view is supported by the observation that overexpression of fructokinase in a mannose-utilizing recombinant strain of *Z. mobilis* results in severe growth retardation (Weisser et al. 1996).

The observed global alterations of phosphorylated pools may result from an elevated fructose 6-phosphate concentration, as described next. Via equilibrium reactions, an increased fructose 6-phosphate level leads to increased concentrations of pentose phosphate pathway intermediates such as ribose 5-phosphate and sedoheptulose 7-phosphate, which were found to be elevated in the ^{31}P extract spectra (assignments tentative). The total of these changes influences some of the enzymes of the Entner-Doudoroff pathway such that the 3-phosphoglycerate levels increase and NDP and NTP pools decrease, as observed. Unfortunately, in the studies reporting their kinetic characterization (Scopes and Griffiths-Smith 1984; Anderson and Dawes 1985; Scopes et al. 1985; Pawluk et al. 1986; Scopes 1997), *Z. mobilis* glycolytic enzymes were not tested for effects of pentose phosphate pathway intermediates. The relative sizes of the NAD(P)(H) pools that are important cofactors for a number of *Z. mobilis* glycolytic enzymes could not be quantitated by either type of ^{31}P-NMR measurements in the present study, thus preventing a more detailed insight into the alterations of reaction equilibria for these enzymes. The nonglycolytic intermediate, dihydroxyacetone phosphate (DHAP), linked with the Entner-Doudoroff pathway via triosephosphate isomerase, also increases as observed in the ^{31}P extract spectra (assignments tentative). This explains the increased formation of dihydroxyacetone and glycerol during fructose metabolism since these two compounds have been shown to originate from dihydroxyacetone phosphate (Horbach et al. 1994). Our hypothesis suggests that overexpression of phosphoglucose isomerase may restore optimal growth and reduce by-product synthesis in fructose-fermenting *Z. mobilis*.

The flux distribution in *Z. mobilis* CP4/pZY228/pZY557*tal* during [1-^{13}C]xylose metabolism as determined in this study revealed strongly altered metabolite fluxes in this strain as compared to the wild-type. Whereas in the latter only as little as 1% of the carbon was metabolized over the pentose phosphate pathway, the recombinant strain was able to metabolize all the xylulose 5-phosphate supplied by the xyloseisomerase and xylulokinase reactions via the heterologous transketolase and transaldolase enzymes. The resulting fructose 6-phosphate and glyceraldehyde-3-phosphate was efficiently metabolized in *Z. mobilis* via the Entner-Doudoroff pathway. In contrast to the hypothesis of Zhang et al. (1995) that possibly the pathway control structure resists a radical alteration of metabolic flux distribution such as is necessary for xylose metabolism in *Z. mobilis*, our analysis showed that the biomass yield on xylose was identical to that on glucose (Table 5) and that the ethanol/carbon dioxide yield was as high as 88% (Table 9). This definitely rules out network misadaptations such as a redox imbalance. The question why the xylose-degrading strain showed growth rates and ethanol productivities that are four- to fivefold reduced in comparison to the wild-type can unequivocally be answered by the results of this study, which show that the in vivo activity of xylulokinase equals the specific activity (i.e. the V_{max}) determined from cell-free extracts. Thus, this enzyme must be rate-limiting, and further attempts to improve the strain should concentrate on increasing its expression level. It can reasonably be expected that if sufficiently high levels of xylulokinase overexpression can be reached, the intracellular levels of xylulose and therewith also of xylose will strongly decrease. This will then lead to a significantly reduced synthesis of xylulose and possibly also of the main by-product, xylitol. In this way, the ethanol yield may rise to 93% (extrapolated from Table 5), almost equivalent to that of fructose metabolism. In fact, an ethanol yield of 92.3% of the theoretical maximum has already been observed in a batch fermentation with the CP4/pZY228/pZY557*tal*

strain (Laufer 1998). The flux analysis furthermore predicted a 6-phosphogluconate dehydrogenase activity of 23 mU/mg protein, which is higher than previously reported values (Feldmann et al. 1992 a) but which should not be considered beforehand as unlikely because the 6-phosphogluconate dehydrogenase assay requires extensive pretreatment procedures of the cell-free crude extract (Feldmann et al. 1992 a) that may influence 6-phosphogluconate dehydrogenase activity.

In conclusion, this study demonstrated for the first time that the differences between glucose and fructose fermentation in *Z. mobilis* relate to a global alteration of the intracellular levels of phosphorylated metabolites in this organism. Furthermore, the rate-limiting step in a recently constructed xylose-degrading recombinant strain was identified as the xylulokinase reaction, and strong evidence was provided that this strain is in principle capable of producing ethanol at specific yields equally as high as those observed for fructose in wild-type *Z. mobilis*.

Acknowledgements We thank S. Bringer for helpful contributions. This research was financed in part by the Volkswagen-Stiftung through the project "Stoffflüsse in *Zymomonas mobilis*".

References

Algar EM, Scopes RK (1985) Studies on cell-free metabolism: ethanol production by extracts of *Zymomonas mobilis*. J Biotechnol 2:275–287

Anderson AJ, Dawes EA (1985) Regulation of glucose-6-phosphate dehydrogenase in *Zymomonas mobilis* CP4. FEMS Microbiol Lett 27:23–27

Barrow KD, Collins JG, Norton RS, Rogers PL, Smith GM (1984) ^{31}P Nuclear magnetic resonance studies of the fermentation of glucose to ethanol by *Zymomonas mobilis*. J Biol Chem 259: 5711–5716

Bringer-Meyer S, Sahm H (1989) Junctions of catabolic and anabolic pathways in *Zymomonas mobilis*: phosphoenolpyruvate carboxylase and malic enzyme. Appl Microbiol Biotechnol 31: 529–536

Bringer-Meyer S, Sahm H (1993) Formation of acetyl-CoA in *Zymomonas mobilis* by a pyruvate dehydrogenase complex. Arch Microbiol 159:197–199

Dawes EA, Large PJ (1970) Effect of starvation on the viability and cellular constituents of *Zymomonas anaerobia* and *Zymomonas mobilis*. J Gen Microbiol 60:31–42

Dawes EA, Ribbons DW (1966) Sucrose utilization by *Zymomonas mobilis*: formation of a levan. Biochem J 98:804–812

Dawes EA, Midgley M, Ishaq M (1970) The endogenous metabolism of anaerobic bacteria. Final technical report (December 1970) for contract no. DAJA 37-67-C-0567, European Research Office, US Army

De Graaf AA, Wittig RM, Probst U, Strohhäcker J, Schoberth SM, Sahm H (1992) Continuous-flow NMR bioreactor for *in vivo* studies of microbial cell suspensions with low biomass concentrations. J Magn Reson Imaging 98:654–659

Feldmann SD, Sahm H, Sprenger GA (1992a) Pentose metabolism in *Zymomonas mobilis* wild-type and recombinant strains. Appl Microbiol Biotechnol 38:354–361

Feldmann SD, Sahm H, Sprenger GA (1992b) Cloning and expression of the genes for xylose isomerase and xylulokinase from *Klebsiella pneumoniae* 1033 in *Escherichia coli* K-12. Mol Gen Genet 234:201–210

Gadian DG (1995) NMR and its applications to living systems, 2nd edn. Oxford University Press, Oxford

Hartbrich A, Schmitz G, Weuster-Botz D, De Graaf AA, Wandrey C (1996) Development and application of a membrane cyclone reactor for *in vivo* NMR spectroscopy with high microbial cell densities. Biotechnol Bioeng 51:624–635

Horbach S, Strohhäcker J, Welle R, De Graaf AA, Sahm H (1994) Enzymes involved in the formation of glycerol-3-phosphate and the by-products dihydroxyacetone and glycerol in *Zymomonas mobilis*. FEMS Microbiol Lett 120:37–44

Kirk K, Raftos JE, Kuchel PW (1986) Triethyl phosphate as an internal ^{31}P NMR reference in biological samples. J Magn Reson Imaging 70:484–487

Laufer B (1998) Erweiterung des Substratspektrums von *Zymomonas mobilis* und Untersuchung Xylose-verwertender Klone. PhD Thesis, Heinrich-Heine-Universität, Düsseldorf, Germany

Low KS, Rogers PL (1984) The macromolecular composition and essential amino acid profiles of strains of *Zymomonas mobilis*. Appl Microbiol Biotechnol 19:75–78

Marx A, De Graaf AA, Wiechert W, Eggeling L, Sahm H (1996) Determination of the fluxes in the central metabolism of *Corynebacterium glutamicum* by NMR spectroscopy combined with metabolite balancing. Biotechnol Bioeng 49:111–129

Marx A, Striegel K, De Graaf AA, Sahm H, Eggeling L (1997) Response of the central metabolism of *Corynebacterium glutamicum* to different flux burdens. Biotechnol Bioeng 56:168–180

Marx A, Eikmanns BJ, Sahm H, De Graaf AA, Eggeling L (1999) Response of the central metabolism in *Corynebacterium glutamicum* to the use of an NADH-dependent glutamate dehydrogenase. Metab Eng 1:35–48

Neidhardt FC, Ingraham JL, Schaechter M (1990) Physiology of the bacterial cell: a molecular approach. Sinauer Associates, Sunderland, Mass

Pawluk A., Scopes RK, Griffiths-Smith K (1986) Isolation and properties of the glycolytic enzymes from *Zymomonas mobilis*. The five enzymes from glyceraldehyde-3-phosphate dehydrogenase through to pyruvate kinase. Biochem J 238:275–281

Reipen IG, Poralla K, Sahm H, Sprenger GA (1995) *Zymomonas mobilis* squalene-hopene cyclase gene (*shc*): cloning, DNA sequence analysis, and expression in *Escherichia coli*. Microbiology 141:155–161

Rogers PL, Lee KJ, Scotnicki ML, Tribe DE (1982) Ethanol production by *Zymomonas mobilis*. Adv Biochem Eng 23:27–84

Rohmer M, Sutter B, Sahm H (1989) Biosynthesis of the side-chain of bacteriohopanetetrol and of a carbocyclic pseudopentose from ^{13}C-labelled glucose in *Zymomonas mobilis*. Eur J Biochem 175:405–411

Schoberth SM, De Graaf AA (1993) Use of *in vivo* ^{13}C nuclear magnetic resonance spectroscopy to follow sugar uptake in *Zymomonas mobilis*. Anal Biochem 210:123–128

Scopes RK (1997) Allosteric control of *Zymomonas mobilis* glucose-6-phosphate dehydrogenase by phosphoenolpyruvate. Biochem J 326:731–735

Scopes RK, Griffiths-Smith K (1984) Use of differential dye-ligand chromatography with affinity elution for enzyme purification: 6-phosphogluconate dehydratase from *Zymomonas mobilis*. Anal Biochem 136:530–534

Scopes RK, Testolin V, Stoter A, Griffiths-Smith K, Algar EM (1985) Simultaneous purification and characterization of glucokinase, fructokinase and glucose-6-phosphate dehydrogenase from *Zymomonas mobilis*. Biochem J 228:627–634

Simon R, Priefer U, Pühler A (1983) Vector plasmids for *in vivo* and *in vitro* manipulations of gram-negative bacteria. In: Pühler A (ed) Molecular genetics of the bacteria-plant interaction. Springer, Berlin Heidelberg New York, pp 98–106

Simpson FJ (1966) D-Xylulokinase. Methods Enzymol 9:454–458

Sprenger GA (1996) Carbohydrate metabolism in *Zymomonas mobilis*: a catabolic highway with some scenic routes. FEMS Microbiol Lett 145:301–307

Sprenger GA, Schörken U, Sprenger G, Sahm H (1995a) Transketolase A of *Escherichia coli* K-12. Purification and properties of the enzyme from recombinant strains. Eur J Biochem 230:525–532

Sprenger GA, Schörken U, Sprenger G, Sahm H (1995b) Transaldolase B of *Escherichia coli* K-12: cloning of its gene, *talB*, and characterization of the enzyme from recombinant strains. J Bacteriol 177:5930–5936

Strohhäcker J, De Graaf AA, Schoberth SM, Wittig RM, Sahm H (1993) ^{31}P Nuclear magnetic resonance studies of ethanol inhibition in *Zymomonas mobilis*. Arch Microbiol 159:484–490

Struch T (1992) Untersuchungen zur Zuckertoleranz in *Zymomonas mobilis*. PhD Thesis, Heinrich-Heine-Universität, Düsseldorf, Germany

Sutter B (1991) Biosynthèse isoprénique chez les procaryotes: un modèle innovateur *Zymomonas mobilis.* PhD Thesis, Université de Haute-Alsace, Mulhouse, France

Swings J, De Ley J (1977) The biology of *Zymomonas*. Bacteriol Rev 41:1–46

Tsolas O, Horecker BL (1972) Transaldolase. In: Boyer PD (ed) The enzymes, 3rd edn, vol 7. Academic Press, New York, pp 259–280

Viikari L (1988) Carbohydrate metabolism in *Zymomonas*. Crit Rev Biotechnol 7:237–261

Viikari L, Korhola M (1986) Fructose metabolism of *Zymomonas mobilis*. Appl Microbiol Biotechnol 24:471–476

Weisser P, Krämer R, Sahm H, Sprenger GA (1995) Functional expression of the glucose transporter of *Zymomonas mobilis* leads to restoration of glucose and fructose uptake in *Escherichia coli* mutants and provides evidence for its facilitator action. J Bacteriol 177:3351–3354

Weisser P, Krämer R, Sprenger GA (1996) Expression of the *Escherichia coli pmi* gene, encoding phosphomannose-isomerase in *Zymomonas mobilis*, leads to utilization of mannose as a novel growth substrate, which can be used as a selective marker. Appl Environ Microbiol 62:4155–4161

Wendisch VF, De Graaf AA, Sahm H (1997) Accurate determination of ^{13}C enrichments in non-protonated carbon atoms of isotopically enriched amino acids by ^{1}H NMR. Anal Biochem 245:196–202

Weuster-Botz D, De Graaf AA (1996) Reaction engineering methods to study intracellular metabolite concentrations. In: Scheper T (ed) Advances in biochemical engineering/biotechnology, vol 54. Springer, Berlin Heidelberg New York, pp 76–108

Wiechert W, De Graaf AA (1996) In vivo stationary flux analysis by ^{13}C labeling experiments. In: Scheper T (ed) Advances in biochemical engineering/biotechnology, vol 54. Springer, Berlin Heidelberg New York, pp 111–154

Wiechert W, De Graaf AA (1997) Bidirectional reaction steps in metabolic networks. 1. Modelling and simulation of carbon isotope labelling experiments. Biotechnol Bioeng 55:101–117

Wiechert W, Siefke C, De Graaf AA, Marx A (1997) Bidirectional reaction steps in metabolic networks. 2. Flux estimation and statistical analysis. Biotechnol Bioeng 55:118–135

Zhang M, Eddy C, Deanda K, Finkelstein M, Picataggio S (1995) Metabolic engineering of a pentose metabolism pathway in ethanologenic *Zymomonas mobilis*. Science 267:240–243